

# Analysis of precursors of tropical cyclogenesis during different phases of the solar cycle and their correlation with the Dst geomagnetic index



Marni Pazos<sup>a,\*</sup>, Blanca Mendoza<sup>b</sup>, Luis Gimeno<sup>a</sup>

<sup>a</sup> Environmental Physics Laboratory, Universidade de Vigo, Ourense 32004, Spain

<sup>b</sup> Instituto de Geofísica, Universidad Nacional Autónoma de México, México D. F. 04510, México

## ARTICLE INFO

### Article history:

Received 27 February 2015

Received in revised form

28 July 2015

Accepted 29 July 2015

Available online 31 July 2015

### Keywords:

Tropical cyclogenesis

Solar activity

Geomagnetic activity

## ABSTRACT

Three tropical cyclogenesis precursors, (absolute vorticity, relative humidity, vertical shear) and the combined Genesis Potential Index are investigated in order to analyse their behaviour during three different phases (descending, minimum and ascending) of the solar cycle. The correlation between these tropical cyclogenesis precursors and the Dst geomagnetic index is also assessed, with the main finding being that the correlations between both the Genesis Potential Index and the vertical shear with the Dst index are statistically significant. This result suggests that the relationship between geomagnetic activity and tropical cyclones might be modulated by the influence of geomagnetic activity on the vertical wind shear.

© 2015 Elsevier Ltd. All rights reserved.

## 1. Introduction

The variability of tropical cyclones (TCs) is of considerable interest, not only because these climate phenomena play an important role in global atmospheric circulation, but also because of the widespread social and economic impacts of their landfall.

In the case of Mexico, its location between the two important basins of the North Atlantic and the Eastern Pacific oceans in which tropical cyclones develop on an annual cycle, make this country of particular interest to climatologists. In the 2013 hurricane season, damage was reported due to strong winds, flooding, and landslides (Beven, 2014; Pasch and Zelinsky, 2013; Brown, 2013) at a total cost off more than 4 billion dollars, more than 3 million people were affected in Mexico alone.

Nowadays, weather forecasting models are able to predict the evolution of TCs a few days before their development, allowing most of the population at risk to be alerted, with the aim to reducing the potential for damages, this being one of the main areas of concern in the study of TCs climatology.

Of the issues that remain unclear in TCs activity, the effect of solar activity have received a fair amount of attention over the past decade and several authors have suggested the existence of such an effect. For instance, Elsner and Jagger (2008), Elsner et al. (2010), Hodge and Elsner (2012), Hodges et al. (2014), linked the number of sunspots with hurricane frequency; Kavlakov and Elsner (2008) found a statically significant correlation between

geomagnetic activity in terms of the Kp index and hurricane intensity over the Atlantic; additionally, several disturbances in geomagnetic activity as well as changes in the number of sunspots and in the intensity of cosmic ray were observed prior to TC genesis by Perez-Peraza et al. (2008).

Mendoza and Pazos (2009), found that the greatest significant correlations occur between Atlantic and eastern Pacific hurricanes and the Dst geomagnetic index. Most importantly, both oceans present the strongest hurricane–Dst relationships during the ascending phases of odd-numbered solar cycles and the descending phases of even-numbered solar cycles (Type 2). Conversely, for the ascending phases of even cycles and the descending phases of odd cycles (Type 1) the relationships are weaker, showing the existence of a 22-year cycle. They also found that Atlantic hurricanes have a negative correlation with the Dst index while Pacific hurricanes have a positive correlation for Type 2 solar cycles. These authors suggested that this behaviour could be due to differences in cyclogenesis and the presence of large-scale climatic phenomena such as the NAO, SOI, etc.

The formation of TCs is related to six averaged parameters (Gray, 1968): the Coriolis parameter ( $f$ ), related to a tropical disturbance developing at least  $5^\circ$  away from the Equator; low-level relative vorticity ( $\zeta$ ); inverse of the tropospheric vertical wind shear (wind shear values below  $10 \text{ ms}^{-1}$  between the surface and upper troposphere); thermal energy of the ocean (sea surface temperature greater than  $26^\circ \text{C}$  up to 60 m below the surface); difference in equivalent potential temperature between the surface and 500 mb (conditional instability); increase of relative humidity in the mid-troposphere (700 mb). In the Atlantic Ocean basin, African easterly waves are considered the main precursor of

\* Corresponding author.

E-mail address: [marnipazos@gmail.com](mailto:marnipazos@gmail.com) (M. Pazos).

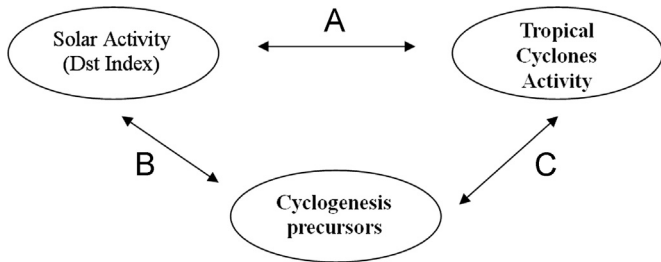


Fig. 1. Framework of the investigation.

TCs (Elsner and Birol, 1999), and their intensity and tracking is being related to certain phases of El Niño/Southern Oscillation (ENSO), the Atlantic Multidecadal Oscillation and the North Atlantic Oscillation (Elsner, 2003). Eastern Pacific tropical cyclogenesis is related to strong easterly waves crossing the mountains of Central America and the presence of low-level monsoon westerlies. TCs frequency in this basin is strongly related with ENSO activity (Camargo et al., 2008).

For this study, we chose atmospheric variables related to some of the parameters mentioned above, namely absolute vorticity ( $\eta$ ), vertical wind shear ( $V_{shear}$ ) and relative humidity ( $\mathcal{R}$ ), according to the availability of data.

Furthermore, as means of approximating the TCs climatology, we calculated the genesis potential index (GPI), developed by Emanuel and Nolan (2004). Several authors have shown evidence of the efficiency of the GPI for modelling TCs climatology (Bruyère et al., 2012; Camargo et al., 2007a, 2007b).

In Fig. 1 is shown the framework of the investigation, the relationship between solar activity, tropical cyclone activity and atmospheric variables linked with tropical cyclogenesis or cyclogenesis precursors (CPs).

Relationship A, was established by Mendoza and Pazos (2009), who proposed the existence of the 22-year hurricane cycle. In the present study, we attempted to establish relationship B, by calculating the correlation between the Dst index and the cyclogenesis precursors (CPs), and relationship C by comparing the GPI index and the cyclogenesis recorded by the National Hurricane Center (NHC) on the first day of a tropical depression, because all the CPs are considered in the calculation of GPI. A secondary objective of this study was to extend the work of Mendoza and Pazos (10) by obtaining the correlation between Dst and the atmospheric variables involved in the genesis of TCs, in order to identify more of the elements involved in the relationship between solar activity and TCs.

2. Data and methodology

Data were obtained from the Earth System Research Laboratory, Physical Division and the National Center for Atmospheric

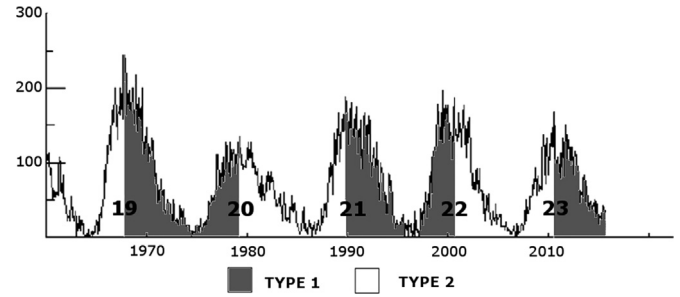


Fig. 3. Sunspot numbers for solar cycles 19–23, separated into Type 1 and 2, respectively.

Table 1  
Periods for Type 1 and Type 2 solar cycles.

Type 1	Type 2
1958–1968	1969–1979
1980–1989	1990–2000
2001–2012	

Table 2  
Three-year composites for each solar cycle.

Period	Descending phase	Minimum phase	Ascending phase	Cycle type
1958–1968	1958–1960	1963–1965	1966–1968	1
1969–1979	1969–1971	1974–1976	1977–1979	2
1980–1989	1980–1982	1984–1986	1987–1989	1
1990–2000	1990–1992	1994–1996	1998–2000	2
2001–2012	2001–2003	2007–2009	2010–2012	1

Research, NOAA-CIRES 20th Century Reanalysis version 2 data. The area under consideration was a grid bounded by 6°–34° N, 120°–10° W, which includes the area of cyclogenesis of the Eastern Pacific and the North Atlantic, with a resolution of 1.5°, and with limits of 1000 and 70 mb of pressure.

The GPI was defined by:

$$GPI = |10^5 \eta|^{3/2} \left(\frac{H}{50}\right)^3 \left(\frac{V_{pot}}{70}\right)^3 (1 + 0.1 V_{shear})^{-2} \tag{1}$$

where  $\eta$  is the absolute vorticity at 850 h Pa ( $s^{-1}$ ),  $\mathcal{R}$  is the relative humidity at 600 h Pa,  $V_{pot}$  is the maximum potential intensity ( $m s^{-1}$ ), and  $V_{shear}$  is the magnitude of the vertical wind shear between 850 h Pa and 200 h Pa ( $m s^{-1}$ ) (Camargo et al., 2007a, 2007b).

The  $V_{pot}$  calculation was made using the MATLAB code available on the Kerry Emanuel's web page.

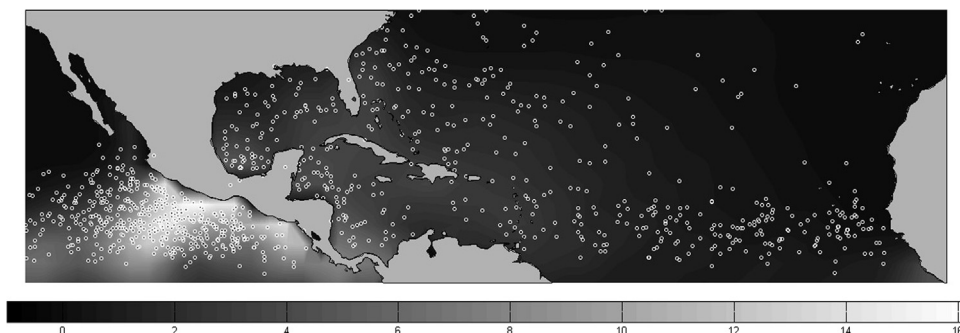
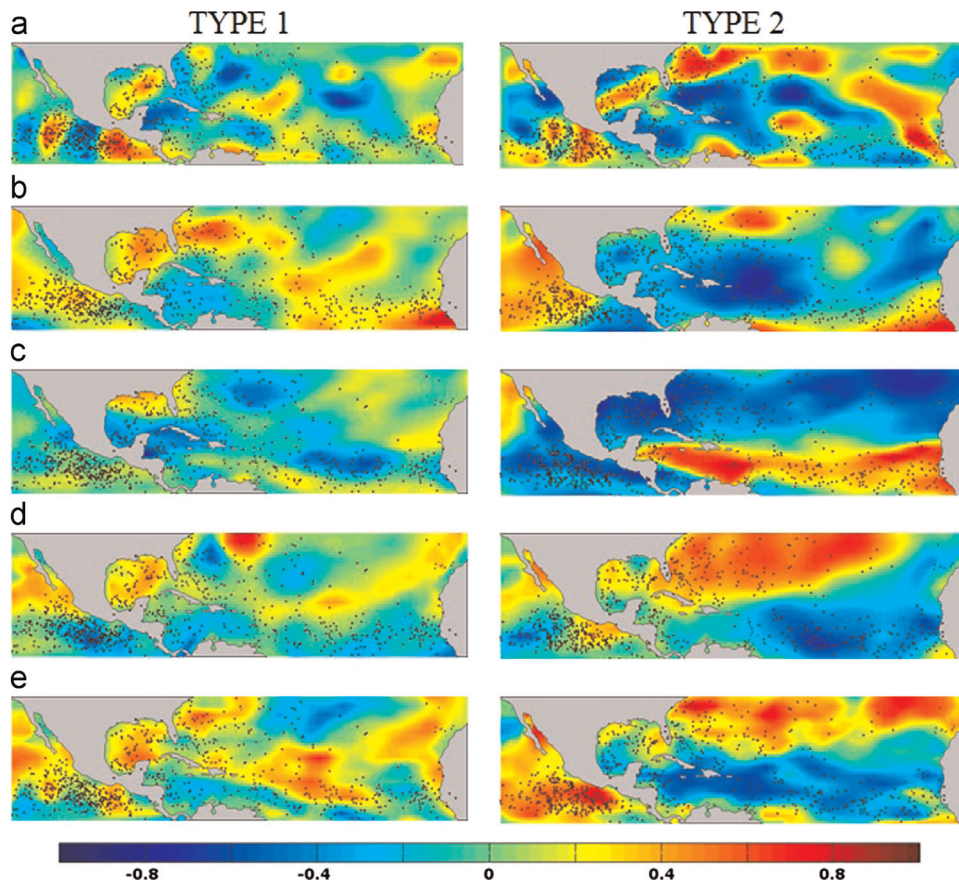
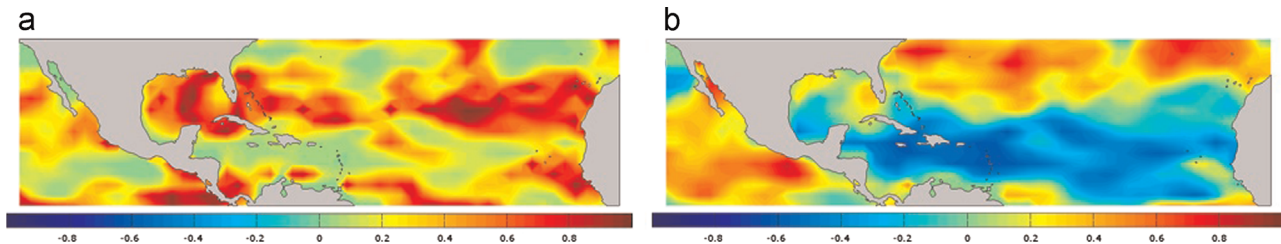


Fig. 2. Tropical cyclogenesis in the North Atlantic and Eastern Pacific basins (white dots), and the GPI values for the period 1957–2012. The bar at the bottom of the figure shows the key used for the shading.



**Fig. 4.** Correlations between the Dst index and variables related to the tropical cyclogenesis precursors: (a) absolute vorticity at 850 h Pa; (b) relative humidity at 600 h Pa; (c) vertical wind shear; (d) maximum potential intensity of winds; (e) GPI for Type 1 solar cycle (left-hand column) and Type 2 solar cycle (right-hand column). All data are annual seasonal averages for the period 1957–2012. The TC climatology for each type of solar cycle is also shown (red dots). (For interpretation of the references to colour in this figure legend, the reader is referred to the web version of this article.)



**Fig. 5.** (a) *P*-values from the GPI–Dst correlation in type 2 solar cycles. Areas of small values (green colour) suggest that the correlation is significant. (b) GPI–Dst correlation in type 2 solar cycles. (For interpretation of the references to colour in this figure legend, the reader is referred to the web version of this article.)

All the variables used to calculate GPI were annual seasonal averages from May to November for the years 1957–2012. Fig. 2 shows the resulting GPI, plotted to allow a comparison with the actual cyclogenesis climatology, in order to assess relationship C (see Fig. 1). The higher values of GPI, represented by lighter shading, coincide with the areas of enhanced cyclogenesis, mainly in the eastern Pacific.

The Dst geomagnetic index is a measurement of disturbances in the Earth's magnetic field, due to solar activity. Data were acquired from the World Data Center in Kyoto, Japan. From these data, we calculated the annual seasonal averages from May to November, 1957–2012, because these months correspond to the annual tropical cyclone season for the region of interest.

The annual means for each time-series were calculated, and the data were classified according to two types of solar cycle. Type 1 are those formed by the descending phase of an even-numbered solar cycle and the ascending phase of an odd-numbered solar cycle, when the interplanetary magnetic field points towards the

Sun, and Type 2 are those formed by the descending phase of an odd-numbered solar cycle and the ascending phase of an even-numbered solar cycle, when the interplanetary magnetic field is directed away from the Sun. Fig. 3 shows the number of sunspots between 1957 and 2010, which correspond to solar cycles 19–23. Type 1 solar cycles are shown in grey and Type 2 solar cycles are shown in white. Table 1 shows the solar cycle periods by type.

An approximation of the relationship between the Dst index and the CPs was found by calculating the correlation coefficients between the average of the seasonal values of each variable and the Dst.

The correlation is calculated by the MATLAB function *corrcoef* in default mode is the Pearson's correlation and defined by the expression :

$$R(x, y) = \frac{C(x, y)}{\sqrt{C(x)C(y)}} \quad (2)$$

where *R* is the correlation coefficient calculated from the input in

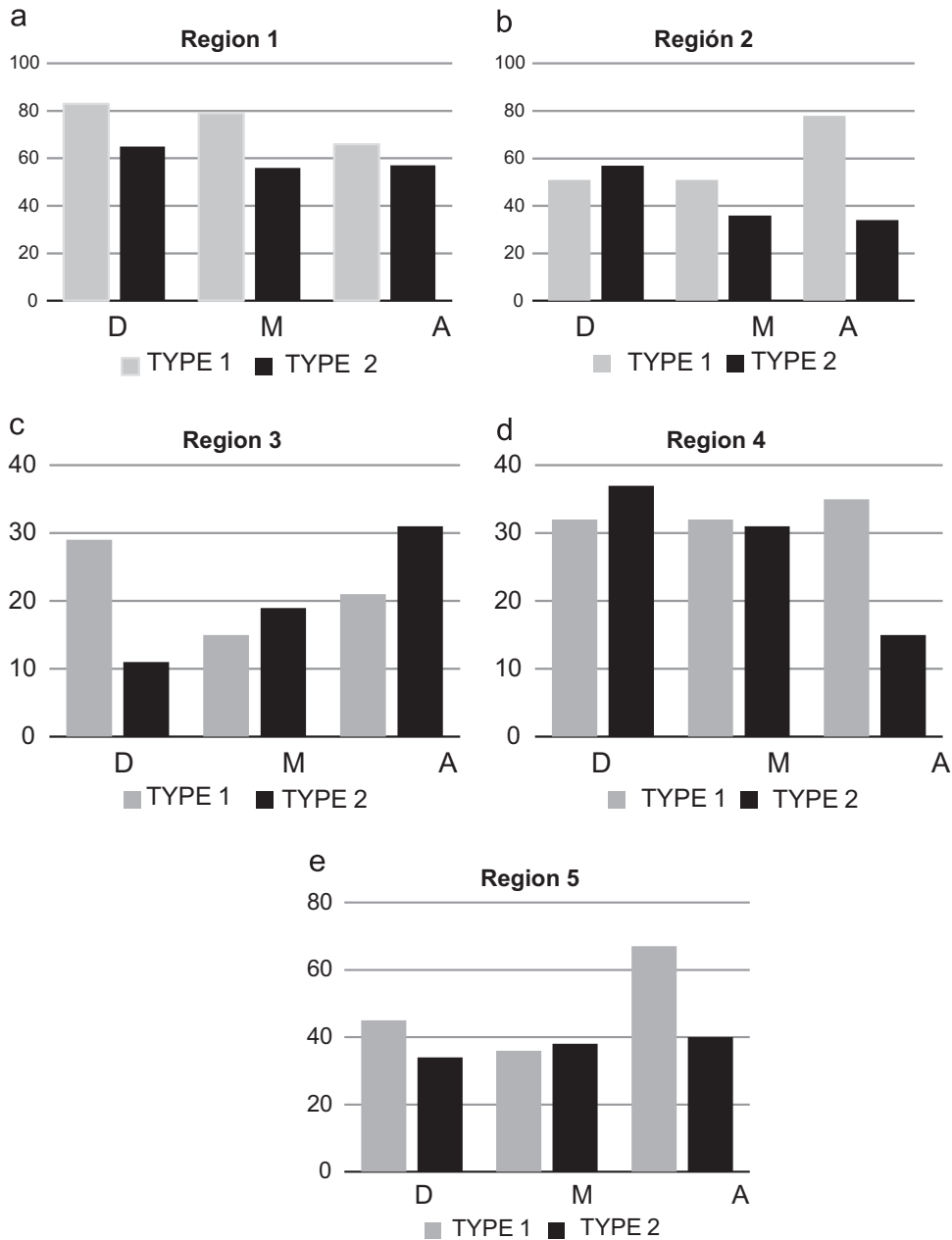


**Fig. 6.** Number of TCs generated for the five regions analysed, shown by solar cycle Type (1 or 2) and for the three different phases of the solar cycle: Descending (D), minimum (M) and Ascending (A).

$x$ ,  $y$ , and  $C$  is a matrix related to the covariance of  $x$  and  $y$  respectively. In this case,  $x$  is Dst and  $y$  the precursor variable. The *corrcoef* function also provides values (*p-values*) for testing the hypothesis of no correlation. Each *p-value* is the probability of getting a correlation as large as the observed value by random chance, when the true correlation is zero. If  $p$  is close to zero, then the correlation  $R(x,y)$  is significant. Tables of critical values of Pearson's correlation for the size of our time series ( $N-2 = 55$ ) with 95% of significance is 0.22.

The correlation was obtained between each of  $\mathcal{H}$ ,  $\eta$ ,  $V_{shear}$ ,  $V_{pot}$  and GPI value on the grid and the Dst yearly mean value, following the same method as that used by Mendoza and Pazos (2009) for the two types of solar cycle. Correlations equal to or higher (lower) than 0.5 ( $-0.5$ ) were considered statistically significant, and the *p-values* where also considered on the results.

To study the time behaviour of the CPs, in each period of the five solar cycles considered in this work (see Table 1), the monthly

anomaly of each variable from May to November was calculated, enabling us to construct composites of three years. Each of the composites corresponded to a different phase of the solar cycle, which we call Descending (D), Minimum (M) and Ascending (A) (see Table 2). For Type 1 solar cycle a time series of nine years was constructed for each phase, and a six-year time series was used for Type 2 solar cycle. The correlation coefficient was again calculated between each CP and the Dst for both time series in the corresponding phase. The analysis was applied to GPI,  $\eta$ ,  $\mathcal{H}$ ,  $V_{pot}$  and  $V_{shear}$ .

### 3. Results and discussion

From the calculation of the correlation coefficient between the Dst index and the CPs, we obtained the results shown on the maps in Fig. 4.

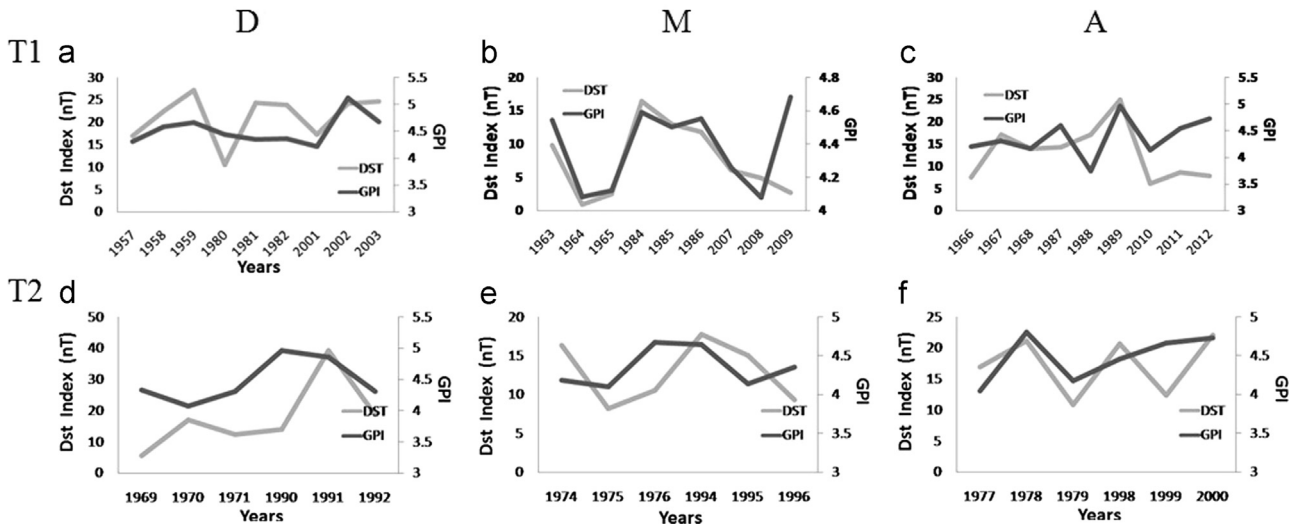


Fig. 7. Dst and GPI. Left-hand column shows values for the D phase of the solar cycle, middle column shows values for the M phase, and right-hand column shows values for the A phase. The first row shows the plots for phases for Type 1 solar cycles and the second row shows the phases for the Type 2 solar cycles.

Significant correlations are those with coefficients higher than 0.5 (from orange to dark red) or less than  $-0.5$  (from blue to dark blue).

Considering first the correlations between Dst and Type 1 cycles in Fig. 4a and 4b (left-hand column), we noticed that there were several areas of significant positive correlation in the Atlantic region. The largest of these correlations are for the absolute vorticity where there are strong positive correlations in the eastern Pacific region, but also a significant negative correlation is also found nearby; there are also some strong positive correlations for relative humidity on the west African coast, and for  $V_{pot}$  there is a very small area in the north Atlantic where the correlations are significant.

A different pattern is shown for Type 2 solar cycles (Fig. 4, right-hand column), with more areas of significant negative correlation. In the case of the vertical wind shear ( $V_{shear}$ ), the significant positive correlation is in a large area between the Caribbean Sea and the west coast of Africa; according to Fig. 2, this is an important area for cyclogenesis. This suggests that when Dst increases, the vertical shear also increases, and the cyclogenesis will be weakened. The opposite occurs northern part of the Gulf of Mexico, in the northwest Atlantic, and in the eastern Pacific. This may also suggest that when Dst increases, and the vertical shear also increases, the area is favourable for cyclogenesis. As shown in Fig. 4e, right-hand column, the GPI has a significant positive correlation with the Dst in the same areas, suggesting also that when the geomagnetic activity increases, the cyclogenesis increases in the eastern Pacific, but decreases in the Atlantic.

Fig. 5a shows the  $p$ -values from the GPI–Dst T2 correlation, along with the correlation values in the right column. (Fig. 5b). Areas of significant positive/negative correlation coincide with those in green colour of  $p$ -values.

The  $p$ -values from all correlations shown in Fig. 4 were analysed in the same form as Fig. 5, but with all other Dst–precursor correlations, and for all areas of significant correlation the  $p$ -value was near to zero, suggesting that the correlation results are reliable.

In order to analyse the spatial patterns and to look more closely at the variations, we focused on five regions with higher probabilities of cyclogenesis. We then compared the TCs climatology of each region, using each of the parameters, during each of the three phases of the solar cycle (D, M and A). We also calculated the correlation between Dst and the CPs by region.

The selected regions were:

- Region 1:  $18^{\circ}$ – $22^{\circ}$  N,  $118^{\circ}$ – $100^{\circ}$  W.
- Region 2:  $8^{\circ}$ – $18^{\circ}$  N,  $100^{\circ}$ – $88^{\circ}$  W.
- Region 3:  $20^{\circ}$ – $30^{\circ}$  N,  $96^{\circ}$ – $84^{\circ}$  W.
- Region 4:  $15^{\circ}$ – $30^{\circ}$  N,  $83^{\circ}$ – $68^{\circ}$  W.
- Region 5:  $8^{\circ}$ – $18^{\circ}$  N,  $62^{\circ}$ – $10^{\circ}$  W.

We also plotted the number of TCs generated in each region, according to the phase of the solar cycle (Fig. 6).

In Fig. 6, for Type 1 solar cycles there is a higher cyclogenesis in the downward stages in regions 1 and 3. In regions 2, 4 and 5, there is a higher cyclogenesis in the ascending stages of the solar cycle. For Type 2 solar cycles, the cyclogenesis is higher in regions 1, 2 and 4 and is lower in regions 3 and 5 in the downward stages of the solar cycle.

We calculated the anomalies of the CPs for each phase of the solar cycle in each of the five regions. The intensity of the anomalies showed no clear variations when comparing them for the different phases of the solar cycle; these variations are therefore not necessarily due to the phase of the solar cycle. However, the correlation coefficient obtained between Dst and the CPs showed significant results particularly for GPI and vertical shear. In Fig. 7, the plotted values of the annual average Dst and the annual average GPI are shown together at the three different phases for the two types of solar cycle.

The values of Dst and GPI in Fig. 7b, have the highest correlation coefficient ( $r = 0.615$ ,  $p$ -value =  $0.078$ ). We then calculated the correlation coefficients between Dst and the CPs, for each of the five regions. The absolute vorticity and relative humidity correlation with the Dst, showed no clear patterns according to solar cycle phase. However, the GPI and vertical shear correlation with Dst, showed an increased correlation coefficient especially in Type 2 solar cycles, as seen in Figs. 8 and 9.

In Figs. 8 and 9, similar patterns for both GPI and vertical shear are found mainly in the D phase of the Type 2 solar cycle. The areas of negative correlation with wind shear are consistent with the areas of positive correlation with GPI in regions 1 and 2, corresponding to the Eastern Pacific cyclogenesis area. The opposite is observed in regions 3, 4 and 5, corresponding to the Atlantic Ocean cyclogenesis area, is very noticeable to the south of region 4, and throughout region 5 in the D phases of Type 2 solar cycles. Fig. 10 shows the plots of average GPI and vertical wind shear for each

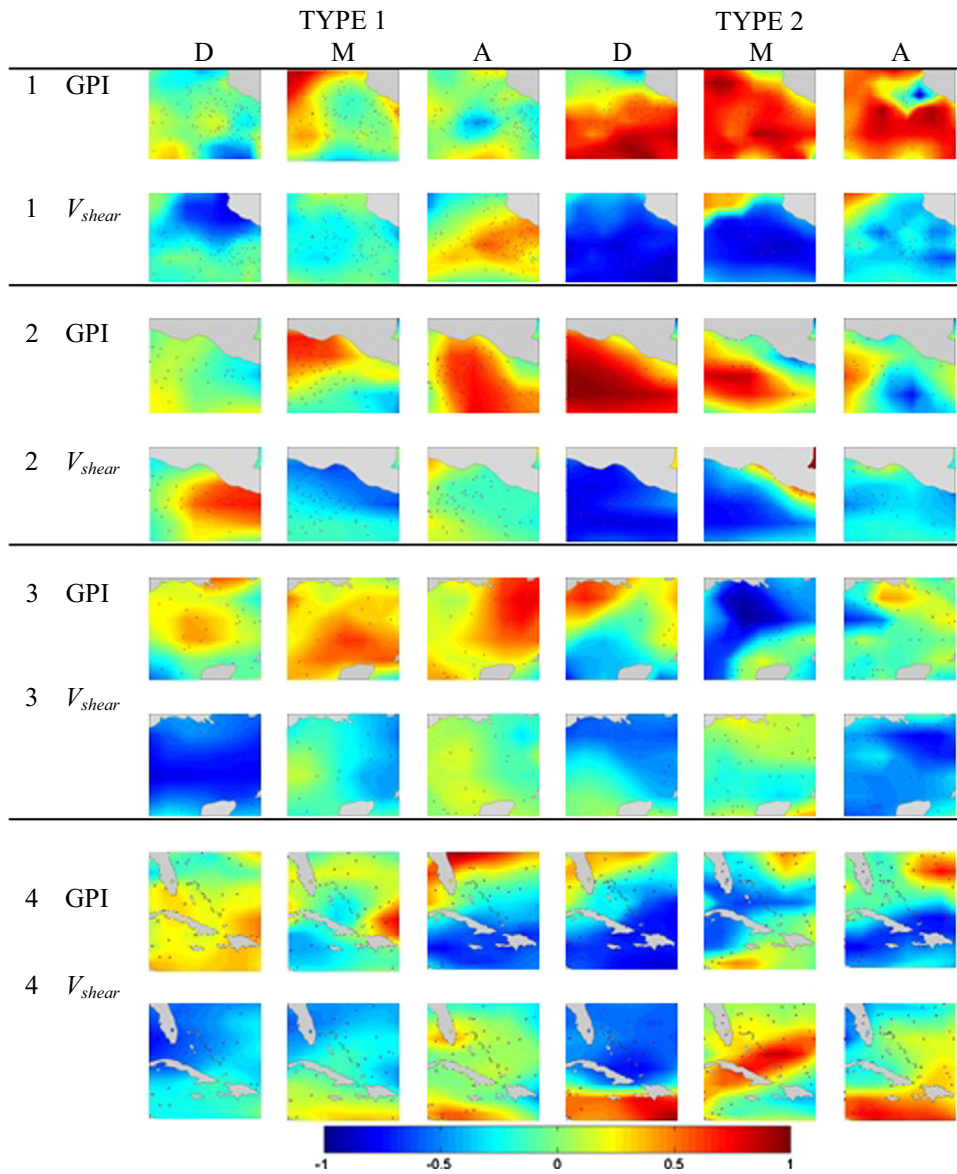


**Fig. 8.** Maps of correlation between Dst and GPI and vertical wind shear ( $V_{shear}$ ) grouped by regions 1, 2, 3 and 4, comparing the patterns of both variables at the same corresponding phase (D, M and A) of the solar cycle (Type 1 and 2) and for the same region. Red dots correspond to cyclogenesis in the same years as the phases of the solar cycles. (For interpretation of the references to colour in this figure legend, the reader is referred to the web version of this article.)

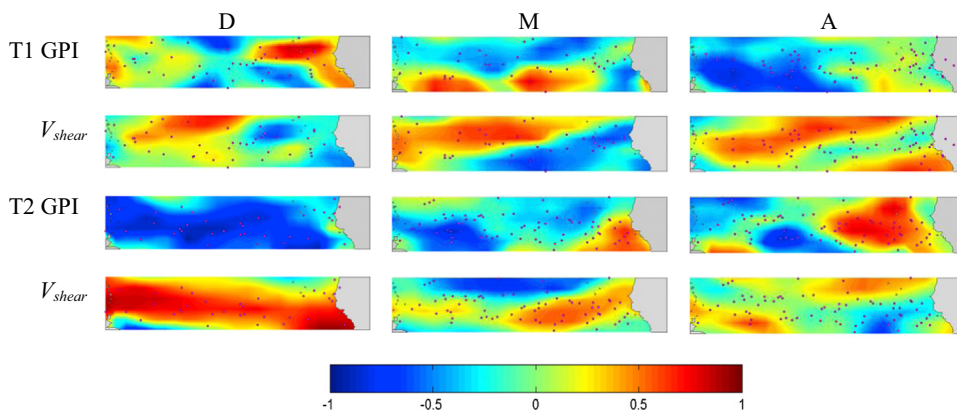


**Fig. 9.** Maps of correlation between Dst and GPI and vertical wind shear ( $V_{shear}$ ) in region 5, comparing the patterns of both variables at the same phase (D, M and A) of the solar cycle (T1 and T2).

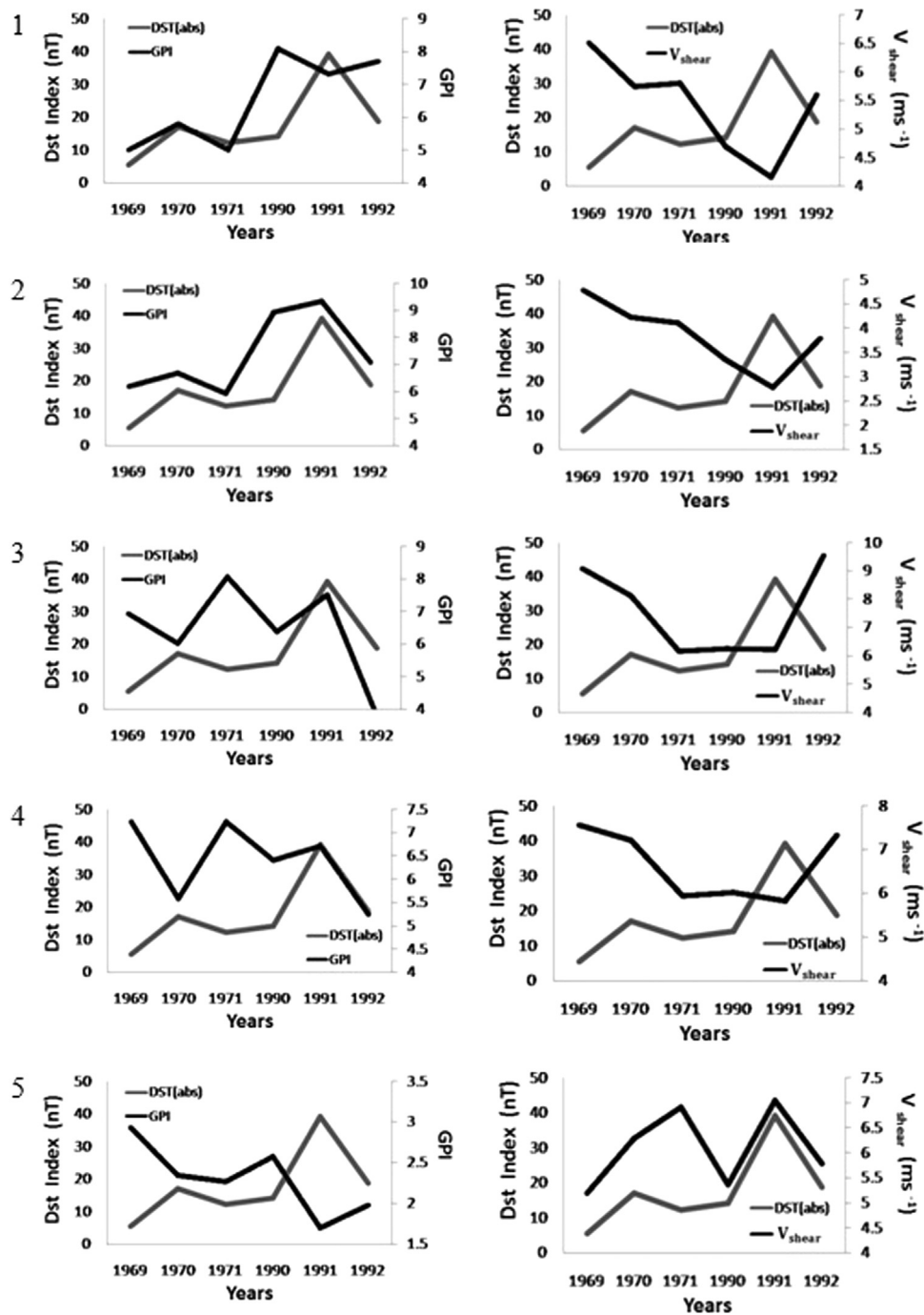


Fig. 10. Plots of GPI and  $V_{shear}$  with Dst in regions 1, 2, 3, 4 and 5 for the D phase of the Type 2 solar cycle.

Table 3

Coefficient of correlation between the Dst index and  $V_{shear}$  for the five regions and the three phases D, M, and A, of Type 1 and 2 solar cycles.

Region :		1	2	3	4	5
T1	D	-0.4051	0.1872	<b>-0.7755</b>	<b>-0.5728</b>	-0.0046
	M	-0.1742	-0.4247	-0.2891	<b>-0.5031</b>	-0.1248
	A	0.1216	0.0015	0.0320	-0.0405	<b>0.5847</b>
T2	D	<b>-0.8198</b>	<b>-0.8537</b>	-0.3771	-0.4885	<b>0.6541</b>
	M	<b>-0.7829</b>	-0.4373	-0.0034	0.4263	-0.0924
	A	<b>-0.7397</b>	-0.4439	<b>-0.5541</b>	0.1241	0.1020

Table 4

Coefficient of correlation between the Dst index and GPI for the five regions and the three phases D, M, and A, of Type 1 and 2 solar cycles.

Region :		1	2	3	4	5
T1	D	-0.1761	-0.0223	0.1438	0.2999	0.1221
	M	0.2101	0.4041	0.4170	-0.0150	-0.1130
	A	0.0238	0.3074	0.4934	0.3024	-0.3634
T2	D	<b>0.5026</b>	<b>0.7164</b>	0.0686	-0.1784	<b>-0.8783</b>
	M	<b>0.6456</b>	-0.0219	<b>-0.8095</b>	0.0250	-0.2236
	A	<b>0.8318</b>	-0.2575	-0.0784	-0.2129	0.0411

region, comparing both to the Dst activity at phase D of the Type 2 solar cycle. Regions 1 and 2 show opposite trends of GPI and  $V_{shear}$  respectively.

The calculation of the correlation between the GPI/ $V_{shear}$  and Dst is shown in Tables 3 and 4.

The highest values of correlation coefficient are in phase D of Type 2 solar cycles, and Region 1 (Eastern Pacific basin) shows a stronger CP–Dst relationship, with significant values in all phases for Type 2 solar cycles. The  $p$ -value in all significant correlations is less than 0.01.

#### 4. Conclusions

These results show that there are significant correlations between CPs and Dst, in agreement with Mendoza and Pazos (2009), and that the strongest CP–Dst relationships can be seen during the ascending phase of odd-numbered solar cycles and the descending phase of even-numbered solar cycles (Type 2 solar cycles). Conversely, for the ascending phase of even-numbered and the descending phase of odd-numbered cycles (Type 1) the correlations are weak, suggesting a probability of the existence of a 22-year cycle, although a longer time series is needed to prove it. In terms of the GPI–Dst relationship, we also found a negative correlation between the Atlantic cyclogenesis and the Dst index, while the Pacific cyclogenesis has a positive correlation for Type 2 solar cycles. Furthermore, we also found that this relationship is more evident during the first three years of solar activity decline in Type 2 solar cycles, consistent with TCs cyclogenesis during the same phases. These results could be proof that tropical cyclogenesis is more affected by disturbances in the Earth's magnetic field as caused by solar activity.

Finally, the relationship found between vertical wind shear and the Dst Index might suggest that the effect of geomagnetic activity on TCs activity is due to an effect that geomagnetic activity has on the vertical wind shear, which is fundamental for TCs development (Gray, 1968; Vecchi and Soden, 2007).

To make these results more robust and reliable, longer time series of these data sets are required, in order to provide greater confidence in the correlations obtained.

Since not only the cyclogenesis precursors defined by Gray are considered in this study, a future work could be to perform a similar analysis with the African Dust. Studies shows the existence of a strong relationship between the TCs activity and the dust transport over the Atlantic (Evan et al., 2006; Prospero and Lamb, 2003). Using some proxies such as African rainfall data to construct a long time series, we could be able to study the relationship between the African Dust as a precursor of TCs activity and solar activity, in order to find mechanisms related to the relationship found in this study.

#### Acknowledgements

This study was supported by CONACyT Grant 204142.

#### References

- Beven, J., 2014. Hurricane Ingrid. National Hurricane Center Tropical Cyclone Report .
- Brown, D.P., 2013. Hurricane Barbara. National Hurricane Center Tropical Cyclone Report.
- Bruyère, C.L., Holland, G.J., Towler, E., 2012. Investigating the use of a genesis potential index for tropical cyclones in the North Atlantic Basin. *J. Clim.* 25, 8611–8626. <http://dx.doi.org/10.1175/JCLI-D-11-00619.1>.
- Camargo, S.J., Emanuel, K.A., Sobel, A.H., 2007a. Use of a genesis potential index to diagnose ENSO effects on tropical cyclone genesis. *J. Clim.* 20, 4819–4834. <http://dx.doi.org/10.1175/JCLI4282.1>.
- Camargo, S.J., Sobel, A.H., Barnston, A.G., Emanuel, K.A., 2007b. Tropical cyclone genesis potential index in climate models. *Tellus A* 59, 428–443. <http://dx.doi.org/10.1111/j.1600-0870.2007.00238.x>.
- Camargo, S.J., Robertson, A.W., Barnston, A.G., Ghil, M., 2008. Clustering of eastern North Pacific tropical cyclone tracks: ENSO and MJO effects. *Geochem. Geophys. Geosyst.* 9, Q06V05. <http://dx.doi.org/10.1029/2007GC001861>.
- Elsner, J.B., Birol Kara, A., 1999. *Hurricanes of the North Atlantic: Climate and Society*. Oxford University Press, p. 488.
- Elsner, J.B., 2003. Tracking hurricanes. *Bull. Am. Meteorol. Soc.* 84, 353–356. <http://dx.doi.org/10.1175/BAMS-84-3-353>.
- Elsner, J.B., Jagger, T.H., Hodges, R.E., 2010. Daily tropical cyclone intensity response to solar ultraviolet radiation. *Geophys. Res. Lett.* 37. <http://dx.doi.org/10.1029/2010GL043091>, issn: 0094-8276.
- Elsner, J.B., Jagger, T.H., 2008. United States and Caribbean tropical cyclone activity related to the solar cycle. *Geophys. Res. Lett.* 35, 0094–8276. <http://dx.doi.org/10.1029/2008GL034431>, issn.
- Emanuel, K., Nolan, D., 2004. Tropical cyclone activity and the global climate system. In: *Proceedings of AMS 26th Conference on Hurricanes and Tropical Meteorology*.
- Evan, A.T., Dunion, J., Foley, J.A., Heidinger, A.K., Velden, C.S., 2006. New evidence for a relationship between Atlantic tropical cyclone activity and African dust outbreaks. *Geophys. Res. Lett.* 33, L19813. <http://dx.doi.org/10.1029/2006GL026408>.
- Gray, W.M., 1968. Global view of the origin of tropical disturbances and storms. *Mon. Wea. Rev.* 96, 669–700.
- Hodges, R.E., Elsner, J.B., 2012. The spatial pattern of the sun-hurricane connection across the North Atlantic. *ISRN Meteorol.* . <http://dx.doi.org/10.5402/2012/517962>
- Hodges, R.E., Jagger, T.H., Elsner, J.B., 2014. The sun-hurricane connection: Diagnosing the solar impacts on hurricane frequency over the North Atlantic basin using a space–time model. *Nat. Hazard.* 73, 1063–1084.
- Kavliakov, S., Elsner, J., Perez-Peraza, J., 2008. Atlantic hurricanes, geomagnetic changes and cosmic ray variations. In: *Proceedings of the 30th International Cosmic Ray Conference*. UNAM, Mexico City, vol. 1, pp. 693–696.
- Mendoza, B., Pazos, M., 2009. A 22-years hurricane cycle and its relation to geomagnetic activity. *J. Atm. Sol.-terrestrial Phys.* 71, 2047–2054.
- Pasch, R.J., Zelinsky, D.A., 2013. Hurricane Manuel. National Hurricane Center Tropical Cyclone Report.
- Perez-Peraza, J., Kavliakov, S., Velasco, V., Gallegos-Cruz, A., Azpra-Romero, E., Delgado-Delgado, O., Villicaña-Cruz, F., 2008. Solar, geomagnetic and cosmic ray intensity changes, preceding the cyclone appearances around Mexico. *Adv. Space Res.* 1601–160
- Prospero, J.M., Lamb, P., 2003. African droughts and dust transport to the Caribbean: climate change implications. *Science* 302, 1024. <http://dx.doi.org/10.1126/science.1089915>.
- Vecchi, G.A., Soden, B.J., 2007. Increased tropical Atlantic wind shear in model projections of global warming. *Geophys. Res. Lett.* 34, L08702. <http://dx.doi.org/10.1029/2006GL028905>.

#### Web reference

<ftp://texmex.mit.edu/pub/emanuel/TCMAX/> (accessed 25.02.15).